Energy Storage and Conversion 2026, 4(3), 4586.
doi: https://doi.org/10.59400/esc4586

Article

Coal fly ash—Municipal solid waste gasification char hybrid electrodes: Pore structure and charge-transport characteristics

Satria Pinandita[1,2,*], Rustam Asnawi[3], Mochamad Syamsiro[4]

[1] Doctoral Program of Engineering Science, Faculty of Engineering, Universitas Negeri Yogyakarta, Yogyakarta 55281, Indonesia
[2] Department of Electrical Engineering, Faculty of Engineering, Universitas Semarang, Semarang 50196, Indonesia
[3] Department of Electrical Engineering Education, Faculty of Engineering, Universitas Negeri Yogyakarta, Yogyakarta 55281, Indonesia
[4] Department of Mechanical Engineering, Faculty of Engineering, Universitas Janabadra Yogyakarta, Yogyakarta 55231, Indonesia
*** Corresponding author:** Satria Pinandita, satriapinandita.2023@student.uny.ac.id

CITATION

Pinandita S, Asnawi R, Syamsiro M. Coal fly ash—Municipal solid waste gasification char hybrid electrodes: Pore structure and charge-transport characteristics. Energy Storage and Conversion. 2026; 4(3): 4586. https://doi.org/10.59400/esc4586

ARTICLE INFO

Received: 29 June 2026
Revised: 21 July 2026
Accepted: 27 July 2026
Available online: 20 August 2026

Abstract: The development of sustainable and cost-effective electrode materials is crucial for advancing metal–air battery technology and reducing dependence on conventional carbon resources. This study explores coal fly ash and Municipal Solid Waste Gasification (MSWG) char as waste-derived electrode precursors, utilizing their mineral-rich and carbonaceous characteristics to improve electrochemical performance. The objectives were to characterize the raw materials' elemental composition and surface functional groups and to comparatively evaluate three hybrid-electrode formulations based on their pore characteristics, electrochemical response, and charge-transfer behaviour. SEM–EDX showed coal fly ash with spherical, microsphere-like particles rich in O, Si, and Al, indicating its role as a mineral-rich silicate and aluminosilicate precursor. MSWG char, however, exhibited irregular, rough, agglomerated morphology with higher carbon content, serving as the main carbon source. FTIR confirmed silicate, oxide, hydroxyl, carbonate, and carbon–mineral bonding. Among the three formulations tested, the formulation containing 20 wt.% coal fly ash (F20) showed the best overall performance, with the highest micropore surface area (1.601 $m^2\ g^{-1}$) and volume (0.0006110 $cm^3\ g^{-1}$). It delivered the largest CV response, energy density of ~208 Wh kg^{-1}, power density of 17.8 W kg^{-1}, and the lowest $\Delta Z'$ of 0.137 Ω. The descriptive results indicate that the measured performance may depend on active-pore accessibility and ion–electron transport characteristics rather than on total BET surface area alone. Further replicated experiments are required to establish the statistical reliability of the observed differences. This study advances waste-ash-derived electrodes for sustainable metal–air battery applications. The novelty of this work is the integrated composition–pore–transport evaluation of directly blended coal fly ash and MSWG char hybrid electrodes.

Keywords: gasification; fly ash; metal-air; pore structure; carbon

1. Introduction

Metal–air batteries have attracted considerable attention because they use oxygen from the surrounding atmosphere as a cathodic reactant and therefore offer potentially high theoretical energy densities [1, 2]. Their practical performance, however, is strongly influenced by the characteristics of the air electrode. An effective air electrode must provide continuous electron-conduction pathways, accessible electrochemical reaction sites, sufficient electrolyte penetration, and efficient oxygen

and ion transport [2–4]. An unsuitable balance among these properties can increase internal resistance, restrict the utilization of active sites, and reduce the attainable energy and power performance [5–7].

Porous carbon materials, including activated carbon, graphite, graphene, and carbon nanotubes, are commonly used in air-electrode systems because they can provide electrically conductive networks and surfaces for electrochemical reactions [3, 4]. Nevertheless, many advanced carbon electrodes require high-purity precursors, chemical activation, catalyst incorporation, or additional structural modification [4, 5]. These preparation requirements can increase production costs and environmental impacts. Consequently, carbonaceous and mineral-containing wastes have increasingly been investigated as alternative electrode precursors for sustainable electrochemical energy-storage systems [8–11].

The electrochemical behaviour of a porous electrode is not determined solely by its total Brunauer–Emmett–Teller surface area. Pore-size distribution, pore accessibility, electrolyte wettability, pore interconnectivity, and ion–electron transport pathways determine how effectively the available surface participates in electrochemical processes [5–7, 12]. Micropores can provide adsorption and charge-storage sites, whereas mesopores facilitate electrolyte penetration and ion transport toward the internal electrode surface [5, 12]. Therefore, an electrode with a high total surface area may still exhibit limited electrochemical performance when its pores are inaccessible or its conductive pathways are interrupted.

Coal fly ash is a coal-combustion residue that generally contains silica, alumina, iron oxides, residual carbon, and other inorganic phases [13–15]. Its particles commonly exhibit spherical or glassy morphologies formed during high-temperature combustion and rapid cooling. Previous studies have investigated fly-ash-derived materials as electrode components, catalyst precursors, and electrocatalytic materials [16–18]. However, the relatively high mineral content of coal fly ash may also introduce electrically resistive domains when it is incorporated in excessive proportions.

Municipal solid waste gasification char is a heterogeneous residue containing residual carbon and mineral components originating from the waste feedstock and gasification process [19–21]. Its carbon content, morphology, and chemical characteristics are influenced by the feedstock composition, gasification temperature, and mineral transformations occurring during treatment. Gasification-derived carbonaceous residues may contribute conductive phases, adsorption sites, and pore structures that support electrochemical processes [9–11]. Thus, MSWG char and coal fly ash may provide complementary functions: MSWG char can serve primarily as a carbon-containing phase, whereas coal fly ash can contribute mineral-rich structural characteristics.

Previous investigations have examined fly-ash-derived electrodes, recovered fly-ash carbon, coal-gasification residues, and other waste-derived carbons for supercapacitors, batteries, oxygen-reduction electrocatalysts, and porous particle electrodes [9–11, 16–18]. Most of these materials were investigated separately or after chemical activation, demineralization, catalytic modification, or other extensive

processing. Limited information is available on the direct blending of mineral-rich coal fly ash with carbon-containing MSWG char and on how their mixing composition simultaneously affects accessible pore characteristics, electrochemical response, and impedance behaviour.

Accordingly, this study investigates hybrid electrodes prepared by directly combining coal fly ash and MSWG char. The morphology, elemental composition, and principal bonding characteristics of the raw materials were examined using scanning electron microscopy coupled with energy-dispersive X-ray spectroscopy and Fourier-transform infrared spectroscopy. Three formulations containing 10, 20, and 30 wt.% coal fly ash, designated F10, F20, and F30, respectively, were evaluated using nitrogen adsorption–desorption analysis, cyclic voltammetry, and electrochemical impedance spectroscopy. These formulations were used as an initial comparative composition-screening series rather than as a Design of Experiments or statistically optimized formulation set.

The principal contribution of this study is the integrated evaluation of raw-material characteristics, electrode composition, accessible pore parameters, cyclic-voltammetry response, and impedance behaviour in directly blended coal fly ash–MSWG char electrodes. Unlike previous studies that used chemically transformed fly ash, isolated carbon fractions, or a single gasification residue, this work combines two different waste-derived materials without extensive chemical processing. The study specifically examines whether electrochemical performance is governed by total surface area alone or by the combined effects of micropore accessibility and ion–electron transport. Therefore, the best-performing formulation is identified only within the investigated F10–F30 range and is not presented as a statistically determined global optimum. The results provide an initial basis for developing waste-derived hybrid electrodes, although full-cell validation, long-term cycling, and practical metal–air battery testing remain necessary in future studies.

The novelty of this study lies in the direct combination of mineral-rich coal fly ash and carbon-containing municipal solid waste gasification char in a controlled hybrid-electrode formulation. Previous studies have mainly investigated chemically modified fly-ash-based electrodes, processed carbon fractions recovered from fly ash, or carbon–mineral electrodes derived from a single gasification residue [9–11,16–18]. In contrast, this study combines two different waste-derived materials and correlates their raw-material characteristics, pore parameters, cyclic-voltammetry response, and impedance behaviour. The contribution of this work is therefore the identification of a composition-dependent pore–transport relationship rather than the demonstration of a fully validated metal–air battery.

2. Materials and methods

The materials used in this study included coal fly ash, municipal solid waste gasification char (MSWG char), commercial graphite powder, NMC 111, polyvinylidene fluoride, N-methyl-2-pyrrolidone, carboxymethyl cellulose, styrene–butadiene rubber, and sodium carbonate. The coal fly ash was collected from the Tanjung Jati B Coal-Fired Power Plant, Jepara, Indonesia, whereas the MSWG

char was obtained from the Putri Cempo Waste-to-Energy Plant, Surakarta, Indonesia. The commercial electrode components were obtained from the suppliers specified in the revised Materials and Methods section.

2.1. Raw-material characterization

An experimental study was conducted to characterize the initial physicochemical properties of coal fly ash and MSWG char before their incorporation into the electrode formulations. Raw-material characterization comprised SEM–EDX analysis of particle morphology and elemental composition and FTIR analysis of the principal functional groups and chemical bonding features.

2.1.1. SEM–EDX characterization of coal fly ash and MSWG char

Coal fly ash and MSWG char were initially dried to remove residual moisture. The dried materials were ground in a ball mill for 3 h and subsequently sieved through a 200-mesh screen to obtain relatively homogeneous powders. After drying, each sample was ground using an iron-ball milling machine for 3 h to obtain a fine and homogeneous powder. The ground samples were then sieved using a 200-mesh sieve. From the sieved powders, 1 gram of coal fly ash and 1 gram of MSWG char were taken for SEM–EDX analysis. SEM–EDX analysis was conducted to observe the surface morphology and elemental composition of the raw materials. SEM was used to identify particle shape, surface texture, and agglomeration characteristics [19], while EDX was used to determine the elemental composition of each sample. The prepared powders were mounted on a sample holder, placed into the SEM chamber, and observed under vacuum conditions. SEM images were collected at magnifications of 500×, 5,000×, 10,000×, and 20,000×. The EDX spectra were then recorded from selected areas to compare the elemental characteristics of coal fly ash and MSWG char.

2.1.2. FTIR characterization of coal fly ash and MSWG

The 200-mesh-sieved coal fly ash and MSWG samples were also used for FTIR analysis. For each test, 1 g of coal fly ash and 1 gram of MSWG char were prepared as representative samples. FTIR analysis was performed to identify the main functional groups and chemical bonding characteristics of the raw materials. The obtained FTIR spectra were then analyzed based on the main absorption bands related to silicate, aluminosilicate, oxide, hydroxyl, carbonate, and carbonaceous groups [22]. The FTIR results were used to support the interpretation of the chemical differences between coal fly ash and MSWG char before electrode fabrication.

2.2. Comparative composition screening of coal fly ash and MSWG char

Coal fly ash and MSWG char were used as waste-derived components in the hybrid electrode powder. The coal fly ash content was varied from 10 to 30 wt.% as an initial composition-screening range. The lower level of 10 wt.% was selected to introduce a mineral-rich fly ash fraction while retaining MSWG char as the dominant carbon-containing component. The upper level of 30 wt.% was selected to examine the effect of a substantially higher mineral fraction while maintaining MSWG char as the majority component of the hybrid powder. An equal increment of 10 wt.% was used to

provide a simple comparison of the composition-dependent trend.

Three formulations, designated F10, F20, and F30, therefore contained 10, 20, and 30 wt.% coal fly ash, respectively. Graphite was maintained at 10 wt.% in all formulations to keep the contribution of the added conductive component constant. Consequently, the MSWG char content decreased from 80 wt.% in F10 to 70 wt.% in F20 and 60 wt.% in F30. The total mass of each hybrid powder formulation was maintained at 60 g.

The investigated compositions were selected for preliminary comparative screening and were not generated using a Design of Experiments, response-surface methodology, or other statistical optimization procedure. Accordingly, the results were used to identify the best-performing formulation only among F10, F20, and F30. They were not intended to establish a statistically determined global optimum in **Table 1**.

Table 1. Composition of the F10, F20, and F30 carbon samples (CS).

Sample	Coal fly ash	Graphite	MSWG char	Total mass
F10	6 g	6 g	48 g	60 g
F20	12 g	6 g	42 g	60 g
F30	18 g	6 g	36 g	60 g

Each prepared sample was then used as the main carbon component in the electrode slurry formulation. The slurry was prepared using CS, MA, SBR, and water + Na_2CO_3. In this formulation, the hybrid powder mixture refers to the F10, F20, or F30 formulation, MA refers to nickel manganese cobalt oxide (NMC), SBR was used as the binder, and water + Na_2CO_3 was added conditionally as the solvent. The slurry formulation is presented in **Table 2**.

Table 2. Electrode slurry formulation for the F10, F20, and F30 samples.

Component	Description	Fraction (%)
CS	Carbon sample (F10/F20/F30)	93.5
MA	Material Active (NMC 111)	2.25
SBR	Styrene-Butadiene Rubber (Binder)	4.25
Water + Na_2CO_3	Solvent	2.5 mL

The cathode slurry was prepared using a CS:MA:SBR ratio of 93.5:2.25:4.25, with NMP added conditionally as the solvent. The anode slurry was prepared using a CS:MA:CMC:SBR ratio of 85:5:3:7, with water added conditionally as the solvent [23]. In both formulations, NMC 111 was used as the added active material, while AB refers to the prepared carbon sample. The cathode was coated on an aluminum current collector with an area of 25 cm × 5.6 cm and a thickness of 0.0045 cm. The anode was coated on a copper current collector with a size of 30 cm × 5.8 cm and a thickness of 0.0085 cm. A total of 2.5 mL Na_2CO_3 solution was used as the electrolyte for each assembled cell. For each formulation, 1.00 g of the hybrid powder mixture was combined with NMC 111 and SBR at the specified mass ratio. The components were mixed until a visually homogeneous slurry was obtained and subsequently coated onto

the designated current collector. The slurry was coated onto the current collector, dried, and then used for BET, CV, and EIS analyses.

2.2.1. Brunauer–Emmett–Teller analysis

BET analysis was conducted using nitrogen adsorption–desorption measurements to determine the specific surface area and pore characteristics of the F10, F20, and F30 electrodes. Prior to analysis, 1 cm × 1 cm electrode samples were degassed to remove moisture and adsorbed impurities. The resulting data were used to calculate the surface area, pore volume, average pore diameter, and micropore contribution of each electrode [4,24].

2.2.2. Cyclic voltammetry (CV) analysis

Cyclic voltammetry was used to evaluate the electrochemical response and charge-storage behaviour of the F10, F20, and F30 electrodes. The CV curves were compared based on their current response and integrated curve area. For CV testing, the cathode was prepared on an aluminium current collector with an area of 25 cm × 5.6 cm and a thickness of 0.0045 cm. The anode was prepared on a copper current collector with a size of 30 cm × 5.8 cm and a thickness of 0.0085 cm. The cathode and anode were assembled into a cell using 2.5 mL Na_2CO_3 electrolyte. The assembled cell was then connected to an electrochemical workstation, and the CV measurement was performed within the selected voltage range. The CV measurement was conducted within a voltage window of 2.4–4.5 V.

The energy–power relationship was further evaluated using a Ragone plot. Ragone plots are commonly used in energy storage studies to compare energy density and power density and to visualize the trade-off between available energy and discharge power [25]. The resulting CV curves were used to compare the electrochemical performance [26] of each sample.

2.2.3. Electrochemical impedance spectroscopy (EIS) analysis

Electrochemical impedance spectroscopy was used to comparatively examine the frequency-dependent impedance responses of the F10, F20, and F30 formulations. The same electrode and cell configuration used for the CV measurements was applied. The electrodes were assembled using 2.5 mL of Na_2CO_3 electrolyte and connected to an electrochemical workstation.

The impedance data were presented as Bode-magnitude, Bode-phase, and Nyquist plots. The plots were compared descriptively to identify differences in the overall impedance magnitude, phase response, and real-impedance range among the formulations. Equivalent-circuit fitting was not performed in the present study. Consequently, physically resolved parameters such as solution resistance (Rs), charge-transfer resistance (Rct), constant phase element parameters, and diffusion impedance were not extracted.

For descriptive comparison, the real-impedance span was calculated as:

$$\Delta Z' = Z'LF - Z'HF$$

where Z′LF and Z′HF are the selected real-impedance values at the low- and high-frequency ends of the measured range, respectively. The calculated $\Delta Z'$ is an

empirical comparison of the variation in Z' over the measured frequency range. It is not equivalent to Rs, Rct, or any other circuit-fitted electrochemical parameter. Separation of ohmic, charge-transfer, non-ideal capacitive, and diffusion contributions would require equivalent-circuit fitting and validation against the complete raw impedance dataset.

2.3. Data analysis

The raw-material and electrode-characterization data were evaluated using a descriptive comparative approach. SEM–EDX images and spectra were examined to compare particle morphology, surface characteristics, and elemental composition, whereas FTIR spectra were interpreted by identifying the principal absorption bands of the raw materials. BET parameters, CV responses, calculated energy–power values, and EIS characteristics were compared among the F10, F20, and F30 formulations.

The dataset available for the present study consisted of one reported measurement series for each formulation and characterization method. Independent experimental replicates sufficient for inferential statistical analysis were not available. Consequently, standard deviations, confidence intervals, and statistical significance tests were not calculated. Differences among F10, F20, and F30 were therefore interpreted as observed descriptive trends and should not be regarded as statistically significant differences.

The formulation showing the most favourable combination of pore characteristics, CV response, energy–power values, and impedance behaviour was identified as the best-performing formulation within the investigated series. Further experiments involving independently prepared electrode replicates are required to quantify experimental variability and confirm the statistical reliability of the observed composition-dependent trends.

The F10–F30 formulation series was treated as an exploratory composition-screening study. No Design of Experiments, response-surface modelling, regression-based optimization, or other statistical optimization method was employed. Consequently, the analysis was limited to a comparative assessment of the three tested formulations. F20 was identified as the best-performing formulation within the investigated range and not as a statistically determined global optimum.

3. Results and discussion

The Results and Discussion section is divided into two main parts: raw-material characterization and comparative electrode-performance evaluation. The comparative formulation results were examined using BET, CV, and EIS measurements of the F10, F20, and F30 electrodes.

3.1. Raw-material characterization

Raw material characterization was carried out to understand the initial properties of coal fly ash and MSWG char before their use in electrode preparation. SEM–EDX analysis was used to observe particle morphology and elemental composition, while FTIR analysis was used to identify the chemical bonding characteristics and dominant

functional groups of each sample.

3.1.1. SEM–EDX characterization of coal fly ash and MSWG char

The coal fly ash particles exhibit a predominantly spherical or microsphere-like morphology, with varying particle sizes (**Figure 1**). This morphology indicates the glassy ash characteristics commonly formed during coal combustion [27]. The SEM–EDX results indicate that coal fly ash is dominated by O, Si, and Al, with a relatively low carbon content. This elemental composition supports the classification of coal fly ash as a mineral-rich precursor, because coal fly ash commonly consists of complex amorphous and crystalline inorganic [28, 29] phases rich in silica, alumina, and metal oxides [11].

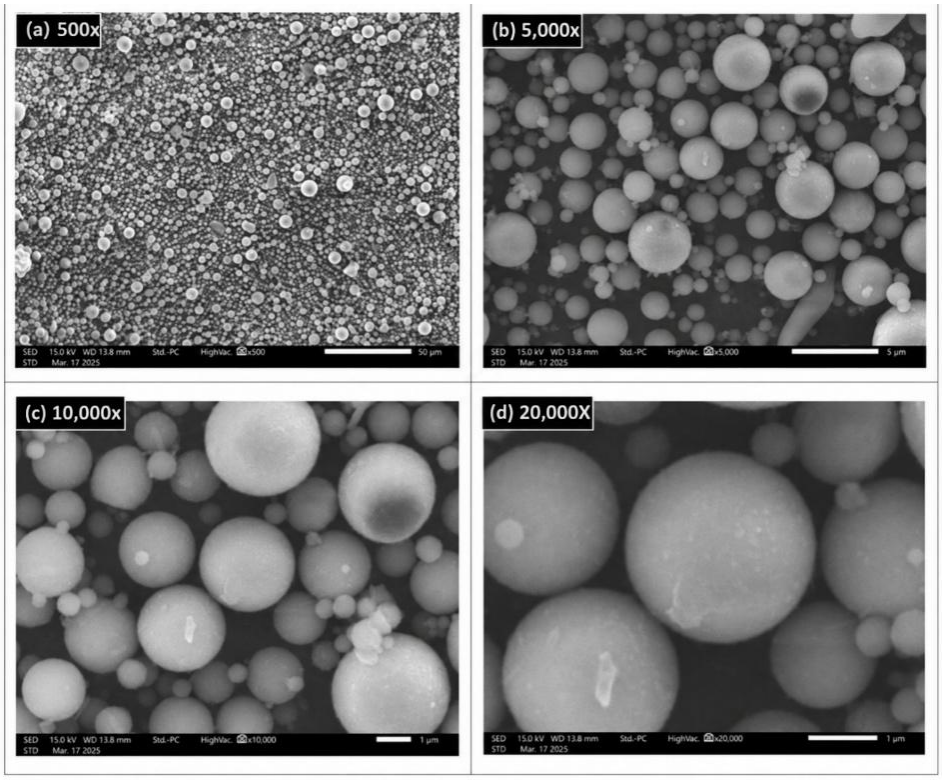

Figure 1. SEM–EDX micrographs and elemental spectra of coal fly ash showing predominantly spherical or microsphere-like particles and mineral-rich characteristics at magnifications of **(a)** 500×, **(b)** 5,000×, **(c)** 10,000×, and **(d)** 20,000×.

In contrast, **Figure 2** shows that MSWG char exhibits irregular, fragmented, rough, and agglomerated particle structures. Unlike the spherical morphology observed in coal fly ash [13], the MSWG char particles appear angular and heterogeneous, indicating the complex nature of municipal solid waste-derived residues [15]. This morphology may result from differences in the original waste composition, thermochemical conversion conditions, and mineral transformation during gasification [30]. The EDX results also show that the carbon content of MSWG char is much higher than that of coal fly ash, reaching approximately 41.21–43.60 mass%. This result indicates that MSWG char acts as the main carbon-containing precursor in the electrode formulation, while coal fly ash contributes mainly mineral-rich silicate and aluminosilicate phases [15].

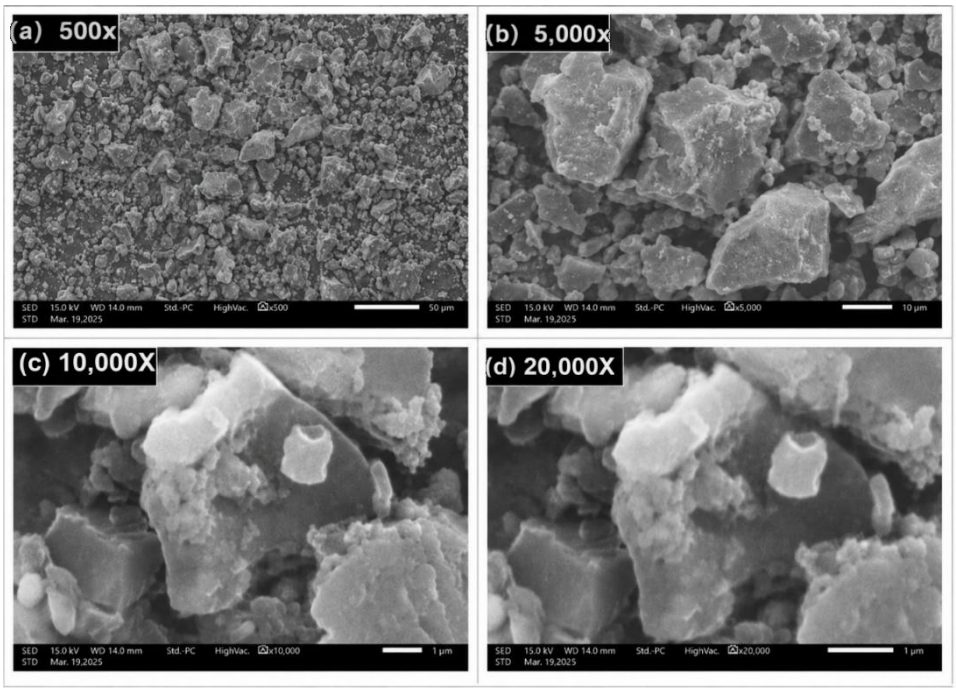

Figure 2. SEM–EDX micrographs and elemental spectra of MSWG char showing irregular, fragmented, rough, and agglomerated particles at magnifications of **(a)** 500×, **(b)** 5,000×, **(c)** 10,000×, and **(d)** 20,000×.

The comparison between **Figures 1** and **2** shows that coal fly ash and MSWG char have different but complementary characteristics. Coal fly ash has smoother, spherical, and glassy particles, which indicate its role as a mineral-rich structural component. This is consistent with previous studies showing that coal fly ash commonly contains spherical aluminosilicate particles and complex amorphous or crystalline mineral phases [11, 13]. In contrast, MSWG char shows rough, irregular, fragmented, and agglomerated particles with higher carbon content. This condition is related to the heterogeneous nature of municipal solid waste and the influence of gasification conditions on the final ash residue [31]. Therefore, coal fly ash may contribute mineral phases for structural stability [15]. MSWG char may provide carbon-containing components that support charge storage and electron transport. This carbon–mineral balance is important because waste-derived carbon materials can support electrode performance through their pore structure, conductivity, and composition [14].

3.1.2. FTIR characterization of coal fly ash and MSWG char

FTIR analysis was used to identify the chemical characteristics of coal fly ash and MSWG char, especially the functional groups related to inorganic and carbonaceous phases. This method is relevant for ash-based materials because FTIR can support SEM–EDX results by identifying silicate-related bonds, inorganic phases, and chemical features that are not fully shown by elemental analysis alone [14]. The FTIR spectrum of coal fly ash showed features related to glassy, silicate-based, and aluminosilicate phases, which is consistent with previous studies reporting that coal fly ash commonly contains amorphous aluminosilicate, crystalline minerals, and glassy silicate components [13, 14].

As shown in **Figure 3**, MSWG char exhibited a more complex FTIR spectrum

associated with its heterogeneous carbonaceous and mineral constituents. This complexity can be related to the heterogeneous composition of municipal solid waste and the effect of gasification conditions, such as temperature, feedstock composition, and mineral transformation [14, 32]. These results indicate that the electrode formulation involves both carbon-containing and inorganic mineral phases. Previous studies on waste-derived carbon electrodes also show that pore structure, electrode composition, and electrode–electrolyte interaction can strongly influence electrochemical behavior. Therefore, the balance between mineral-rich coal fly ash and carbon-containing MSWG char is important for controlling pore development, electrolyte accessibility, and charge-transport behavior in the final electrode structure [5,33].

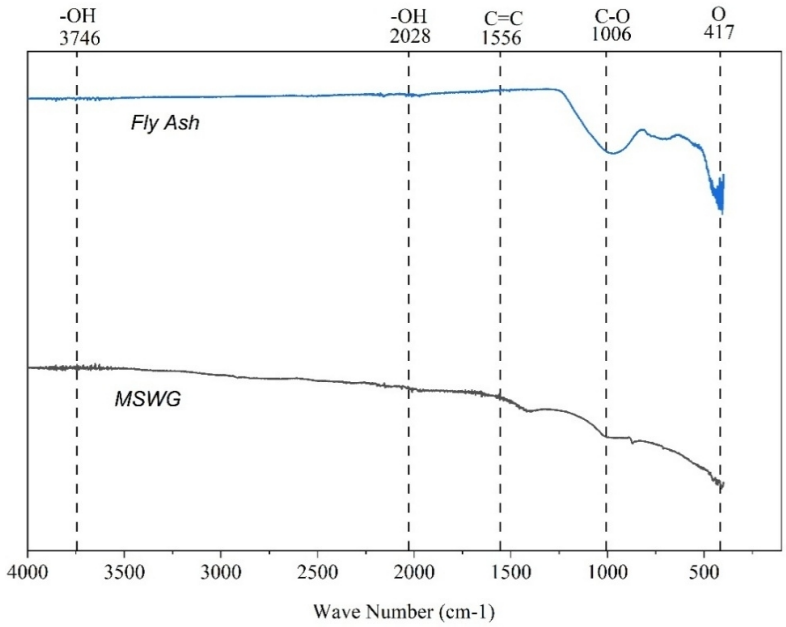

Figure 3. FTIR spectra of coal fly ash and MSWG char showing the dominant silicate-related characteristics of coal fly ash and the carbonaceous–mineral features of MSWG char.

3.2. Composition-dependent performance of coal fly ash–MSWG char electrodes

The F10, F20, and F30 samples were prepared to evaluate the effect of coal fly ash and MSWG char composition on electrode performance. Coal fly ash was used as the mineral-rich component, while MSWG char was used as the main carbon-containing component.

Pore structure of the F10, F20, and F30 based on bet analysis

BET analysis was conducted to evaluate the pore structure and surface characteristics of the F10, F20, and F30 electrodes. The main parameters analyzed were BET specific surface area, total pore volume, micropore surface area, micropore volume, and average pore diameter. These parameters were used to determine which composition provided the most favorable pore structure for ion accessibility and charge storage. The BET results are summarized in **Table 3**.

Table 3. Main BET parameters of the F10, F20, and F30 samples.

Sample	S_{BET} (m^2 g^{-1})	V_{total} (cc g^{-1})	S_{micro} (m^2 g^{-1})	V_{micro} (cc g^{-1})	D_{avg} (nm)	Interpretation
F10	8.375	0.05360	1.283	0.0004368	25.60	Highest total surface area.
F20	6.727	0.04801	1.601	0.0006110	28.55	Highest micropore contribution
F30	6.844	0.04743	0.8054	0.0002737	27.72	Sharp decrease in micropore contribution

Note: The reported values represent individual measurements for each formulation. Independent experimental replicates were not available; therefore, the values are presented without standard deviations or confidence intervals and are interpreted descriptively.

The individual measurements presented in **Table 3** show an observed difference in the pore characteristics of the three formulations. F10 exhibited the highest measured total BET surface area, whereas F20 exhibited the highest measured micropore surface area and micropore volume. Within the present dataset, this pattern suggests that total surface area alone may not adequately describe the pore characteristics relevant to electrochemical accessibility. However, because independently prepared replicates were not examined, the magnitude and statistical significance of these differences could not be determined. The results should therefore be interpreted as preliminary composition-dependent trends requiring confirmation through replicated experiments [7]. All samples show average pore diameters in the mesoporous range, with values of 25.60, 28.55, and 27.72 nm for F10, F20, and F30, respectively. This pore range is beneficial because mesopores can support electrolyte penetration [34] and ion transport, while micropores contribute to charge-storage sites [35]. Therefore, the combination of higher micropore contribution and mesoporous pathways in F20 suggests a more favorable pore structure for electrochemical performance [12].

Among the individual measurements obtained in this study, F20 showed the most favorable combination of micropore surface area, micropore volume, and average pore diameter. This observation indicates a potentially more effective contribution of accessible pores at the intermediate coal fly ash fraction. Nevertheless, the available data do not establish that the differences among F10, F20, and F30 are statistically significant. Accordingly, F20 is described as the formulation with the most favorable measured pore characteristics within the present screening series, rather than as a statistically verified superior formulation. Although its total BET surface area is not the highest, its higher S_{micro} and V_{micro} suggest that the intermediate composition between coal fly ash and MSWG char promotes a more effective active-pore contribution. This condition is important because carbon pores do not contribute equally to electrochemical performance; their size, shape, accessibility, and connection to the electrolyte pathway directly affect charge storage and power response [5]. In contrast, F30 shows a clear decrease in micropore contribution despite having a slightly higher S_{BET} than F20. This result suggests that excessive coal fly ash addition may increase the contribution of mineral-rich domains, which could reduce the formation or accessibility of active micropores [5]. For waste-ash-derived electrodes, this interpretation is reasonable because carbonaceous and inorganic mineral phases coexist [11] within the material and may jointly influence pore development, electrolyte accessibility, and charge-transport behavior [36].

3.2.1. CV response and energy–power performance

Figure 4 Cyclic-voltammetry curves obtained from one measurement series for each of the F10, F20, and F30 formulations. Solid lines represent the forward potential scan, whereas dashed lines represent the reverse potential scan. The curves are presented for descriptive comparison and do not include variability estimates from independent experimental replicates.

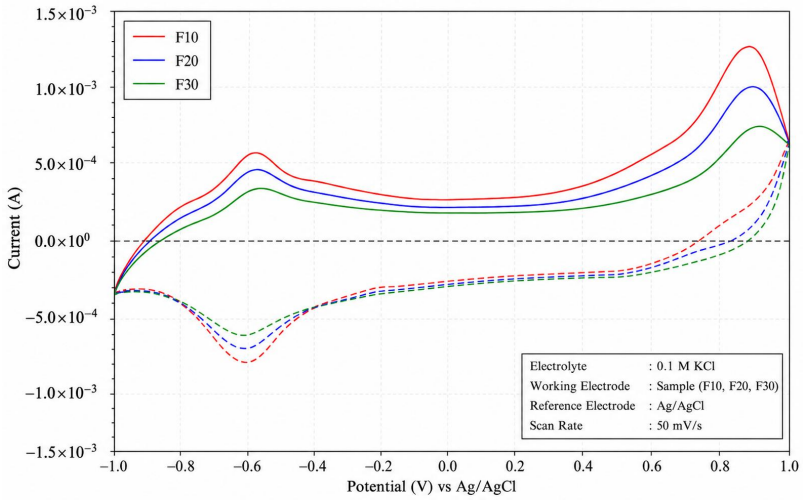

Figure 4. Cyclic-voltammetry curves of the F10, F20, and F30 formulations.
Note: Solid lines represent the forward potential scan, whereas dashed lines represent the reverse potential scan.

Figure 4 shows that F20 produced the largest measured CV response among the three formulations. This observation is consistent with its higher measured micropore surface area and micropore volume, which may facilitate ion accessibility and utilization of electrochemically active sites. F30 produced a lower measured CV response and contained a higher coal fly ash fraction. However, because only one measurement series was available for each formulation, these differences represent descriptive observations rather than statistically significant differences. The proposed relationships among composition, pore accessibility, and CV response therefore require confirmation using independently prepared replicate electrodes.

Figure 5 the combined cyclic voltammetry curves of F10, F20, and F30 measured within the voltage range of 2.4–4.5 V. Among the three samples, F20 exhibits the largest CV area and the strongest current response, indicating superior charge-storage capability and more effective utilization of active sites. Although F10 has the highest BET surface area, its CV area is smaller than that of F20. This result further confirms that the total surface area is not the sole determining factor for electrochemical performance.

Figure 5 presents the Ragone plot comparing the energy density and power density of the F10, F20, and F30 electrodes. F20 delivers the highest combined energy–power performance, with an energy density of approximately 208 Wh kg^{-1} and a power density of approximately 17.8 W kg^{-1}. These values are higher than those obtained for F10 and F30, indicating that the intermediate composition provides the most effective balance among carbon contribution, active pore availability, and charge-transport efficiency [5].

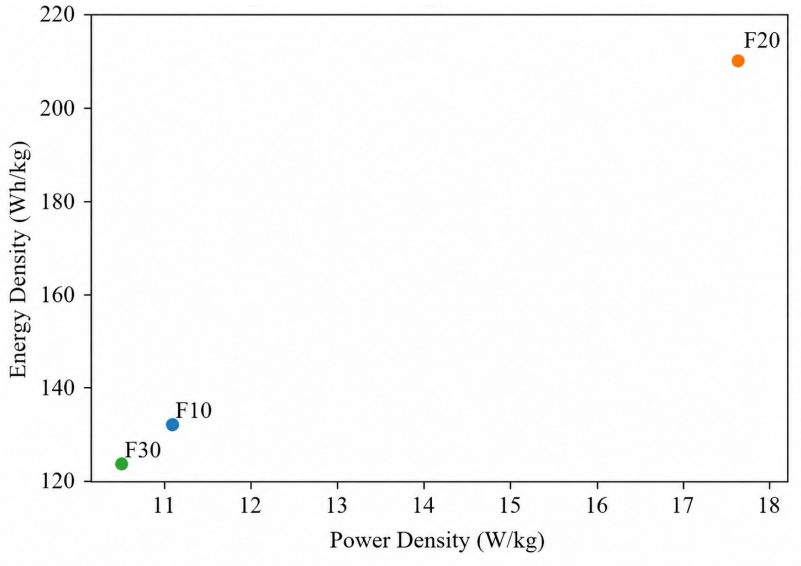

Figure 5. Ragone plot comparing the calculated specific energy and specific power of the F10, F20, and F30 formulations.

Figure 5 shows that F20 had the highest calculated specific energy and specific power among the three individual datasets. This observation is consistent with its comparatively high micropore contribution and CV response. F10 had a higher total BET surface area but lower calculated energy and power values, whereas F30 showed lower calculated values and substantially higher impedance. These results suggest a possible relationship among accessible pores, composition, and charge transport. Nevertheless, no statistical inference can be made because independently prepared replicate electrodes were not evaluated.

Overall, the CV and Ragone results show that F20 performed best within the investigated F10–F30 formulation range [13]. Its improved response was not associated with the highest total BET surface area but with a more favourable combination of active pore characteristics and charge transport [15, 30]. However, the present results do not establish F20 as a global optimum because only three discrete compositions were investigated and no statistical optimization procedure was employed. The observed trend instead indicates that future formulation development should examine pore–transport balance using additional intermediate and extended coal fly ash fractions.

3.2.2. Descriptive EIS response and real-impedance span

Figure 6 presents the Bode-magnitude plots of the F10, F20, and F30 formulations. F30 exhibited a substantially higher impedance magnitude than F10 and F20 over most of the measured frequency range. This result indicates that the tested F30 cell had greater overall opposition to the applied alternating-current signal. However, the Bode-magnitude plot alone cannot separate the contributions of electrolyte resistance, interfacial charge transfer, non-ideal capacitance, and diffusion. Therefore, the higher impedance of F30 is reported as an observed composition-dependent impedance response rather than as evidence of a particular equivalent-circuit element or transport mechanism.

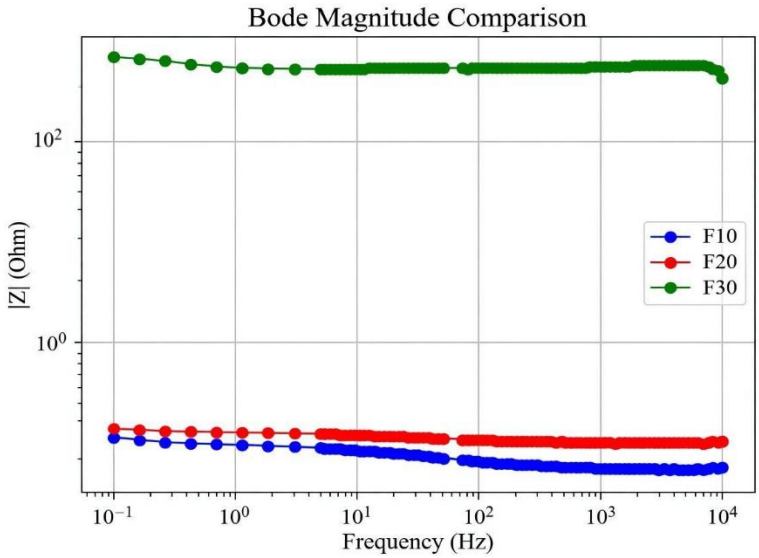

Figure 6. Bode-magnitude plots of the F10, F20, and F30 formulations.

The higher impedance of the F30 can be associated with the increased fraction of coal fly ash in the electrode formulation. Since coal fly ash is mainly composed of mineral-rich inorganic phases [17], Excessive fly ash content may increase the proportion of resistive domains [17] within the electrode structure. This condition may reduce the continuity of conductive pathways and limit electrolyte access to active pores [37]. Previous studies on porous electrodes have shown that impedance behavior is strongly affected by the distribution of resistive, capacitive, and diffusion-related processes within the electrode structure [38].

Figure 7 presents the Bode-phase responses of the three formulations. F10 and F20 exhibited broadly comparable phase-angle variations, whereas F30 showed a flatter phase response over much of the frequency range. These differences indicate that the formulations produced different frequency-dependent electrochemical responses. Nevertheless, individual resistive, capacitive, and diffusion processes cannot be assigned quantitatively from the phase plots without equivalent-circuit fitting. The phase results are therefore interpreted qualitatively.

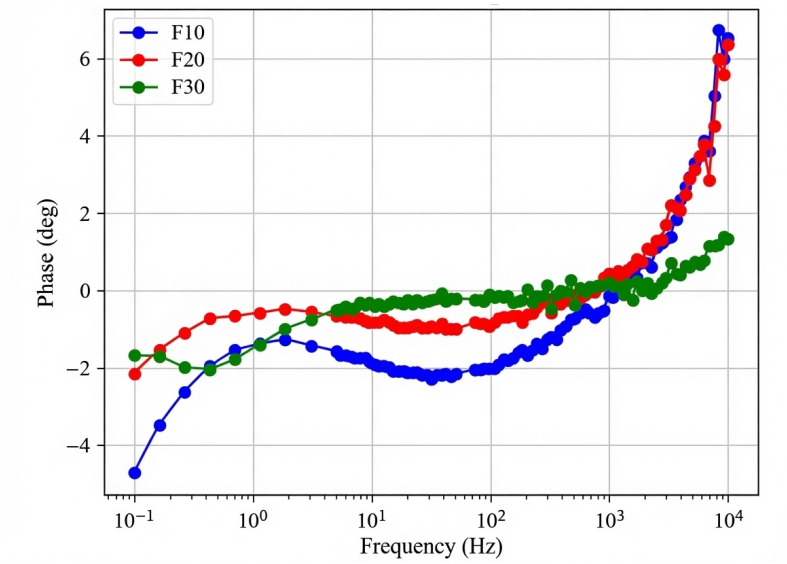

Figure 7. Bode-phase plots of the F10, F20, and F30 formulations.

Figure 8 presents the Nyquist plots of the F10, F20, and F30 formulations. The F30 data were positioned at substantially higher Z′ values than the F10 and F20 data, indicating a higher overall measured real impedance for the tested F30 cell. The selected high- and low-frequency Z′ values were used to calculate the descriptive ΔZ′ values presented in **Table 4**.

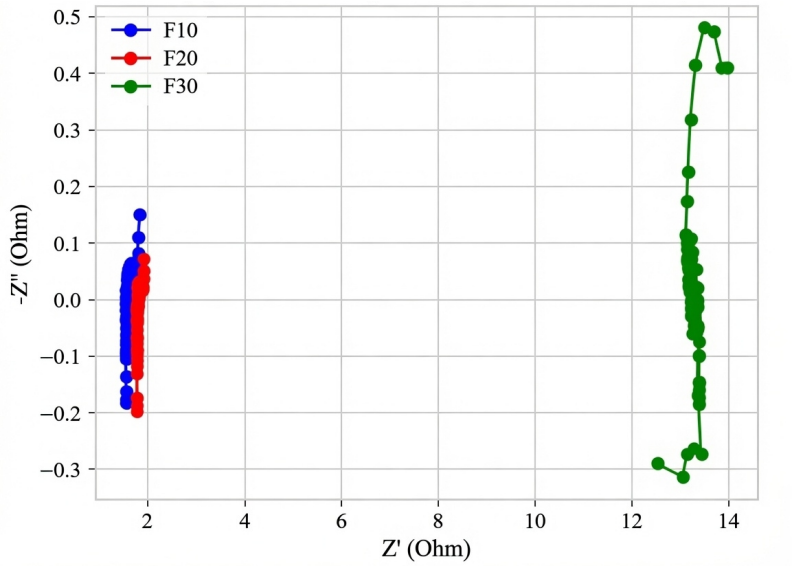

Figure 8. Nyquist plots of the F10, F20, and F30 formulations.

Table 4. Preliminary estimation of EIS parameters from Nyquist plots before equivalent circuit fitting.

Sample	Selected high-frequency Z′ (Ω)	Selected low-frequency Z′ (Ω)	ΔZ′ (Ω)	Descriptive observation
F10	1.548	1.826	0.278	Lowest absolute Z′ values among F10 and F20, with an intermediate ΔZ′.
F20	1.777	1.914	0.137	Smallest ΔZ′ among the three tested formulations.
F30	12.520	13.980	1.460	Highest absolute Z′ values and largest ΔZ′.

Note: ΔZ′ was calculated as Z′LF − Z′HF for descriptive comparison only. The selected high-frequency Z′ value was not treated as Rs, and ΔZ′ was not treated as Rct. Rs, Rct, CPE, and diffusion parameters were not extracted because equivalent-circuit fitting was not performed.

F20 exhibited the smallest ΔZ′, at approximately 0.137 Ω, compared with 0.278 Ω for F10 and 1.460 Ω for F30. However, F10 had slightly lower absolute Z′ values at both selected endpoints than F20. Therefore, the present EIS results do not independently demonstrate that F20 had the lowest total resistance or the lowest charge-transfer resistance. They show only that F20 had the smallest variation in Z′ between the selected endpoints, whereas F30 had both the highest absolute Z′ values and the largest ΔZ′.

Because no equivalent circuit was fitted, the high-frequency value cannot be formally reported as Rs, and ΔZ′ cannot be reported as Rct. The EIS results are therefore used only for descriptive comparison with the BET and CV observations [5, 6, 39] in **Table 4**.

The EIS measurements are consistent with the trends observed in the CV curves and Ragone plot. F20 showed the smallest measured ΔZ′, whereas F30 showed a

substantially higher impedance response. These individual measurements suggest that the F20 formulation may provide more favorable charge-transport characteristics within the investigated series. However, the absence of independent replicate electrodes prevents assessment of measurement variability and statistical significance. Therefore, the EIS results support only a preliminary descriptive interpretation and should not be regarded as statistical confirmation of differences among the formulations [8, 17, 39]. Therefore, the high impedance response of F30 supports the conclusion that excessive mineral-rich precursor content is less favorable for charge transport in coal fly ash/MSWG char-derived carbon electrodes.

3.2.3. Correlation among BET, CV, and EIS results and comparison with previous studies

In **Table 5**, although a high S_{BET} provides more exposed surface sites, excessively high surface areas dominated by narrow micropores can impede ion transport and oxygen accessibility, increase internal resistance, and promote flooding effects, thereby deteriorating the overall performance of metal–air battery electrodes [40]. The characterization results show that coal fly ash and MSWG char have different roles in the electrode formulation. Based on SEM–EDX and FTIR analyses, coal fly ash mainly acts as a mineral-rich precursor, as shown by its spherical/microsphere-like morphology and the dominance of O, Si, and Al elements. This finding is consistent with previous studies reporting that coal fly ash commonly contains glassy, silicate, aluminosilicate, and metal oxide phases, which can be identified through SEM–EDX and FTIR characterization [13,15]. In contrast, MSWG char showed irregular and agglomerated particles with a much higher carbon content of approximately 41.21–43.60 mass%, compared with only 3.91–4.74 mass% in coal fly ash. This result supports the role of MSWG char as the main carbon-containing precursor, while coal fly ash contributes mineral-based structural features. Previous studies have also shown that municipal solid waste gasification residues generally have complex compositions due to variations in waste feedstock, gasification conditions, mineral transformation, and residual carbon content [41]. Therefore, the SEM–EDX and FTIR results confirm that the combination of coal fly ash and MSWG char provides a useful carbon–mineral balance for electrode design.

Table 5. Correlation among pore structure, CV response, and charge-transport behavior.

Parameter	Electrochemical relevance	F10	F20	F30	Relevance to novelty
S_{BET}	The higher the number of available active sites, the better.	Highest	Moderate	Moderate	Surface area is not the sole determinant of performance.
S_{micro}	Charge storage and adsorption.	Moderate	Highest	Lowest	Effective micropores are important for ion accessibility.
CV area	The greater the storage capacity, the greater the charge transfer.	Moderate	Highest	Low	F20 shows the best utilization of active sites.
Energy-power	The greater the amount of energy that can be stored, the better.	Moderate	Highest	Low	F20 delivers the highest overall electrochemical performance.
EIS	The shorter the ion transport, the faster.	Low impedance	Low and efficient impedance	Very high impedance	F30 suffers from significant transport resistance.

The energy and power performance summarized in **Table 5** further confirms the superior electrochemical behavior of F20. Although F10 possesses the highest BET

surface area, its energy and power densities are lower than those of F20. This indicates that the available surface area in F10 was not fully utilized for charge storage. In contrast, F20 delivers the highest energy density of approximately 208 Wh kg^{-1} and power density of approximately 17.8 W kg^{-1}, suggesting that this composition provides the most favorable balance between active pore accessibility and charge-transport efficiency. Meanwhile, F30 shows lower energy and power densities, which may be attributed to increased transport resistance caused by the higher fraction of mineral-rich fly ash.

The optimization results from BET, CV, Ragone, and EIS analyses confirm that F20 is the most balanced composition among the investigated electrodes. F10 BET of 8.375 m^2 g^{-1}, but it did not deliver the best electrochemical performance. In contrast, F20 had the highest micropore surface area and micropore volume, reaching 1.601 m^2 g^{-1} and 0.0006110 cm^3 g^{-1}, respectively, followed by the largest CV response and the highest energy–power performance of approximately 208 Wh kg^{-1} and 17.8 W kg^{-1}. EIS analysis also showed that F20 had the smallest $\Delta Z'$ value of 0.137 Ω, compared with 0.278 Ω for F10 and 1.460 Ω for F30, indicating more efficient charge transport. These findings are in line with previous studies showing that electrochemical performance in porous carbon electrodes is not governed solely by total surface area, but also by pore size distribution, micropore–mesopore balance, electrolyte accessibility, and ion–electron transport pathways [5, 7, 12]. Meanwhile, the lower performance and higher impedance of F30 suggest that excessive coal fly ash may increase resistive mineral-rich domains and limit active pore accessibility. Therefore, the main finding of this study is that the optimization of coal fly ash/MSWG char-derived carbon electrodes should focus on pore–transport synergy rather than only increasing BET surface area, which is consistent with studies emphasizing pore-structure control and charge-transport connectivity as key design parameters for energy-storage electrodes [6,7,42].

Previous studies have demonstrated that coal fly ash and gasification residues can be converted into electrochemical materials through several approaches. Wang et al. [16] transformed fly-ash-derived components into cobalt–iron silicate for supercapacitor applications, whereas Fernandes et al. [17] and Nunes et al. [18] focused on carbon-rich char recovered from fly ash for oxygen-reduction applications. Other studies used residual carbon from coal gasification as an oxygen-reduction catalyst [31] or combined carbon and mineral phases originating from a single coal gasification fine-slag source [16].

The material strategy used in the present study differs from these approaches. Coal fly ash was not chemically transformed into a new silicate phase, and the carbon fraction was not isolated, demineralized, or graphitized. Instead, mineral-rich coal fly ash and carbon-containing MSWG char from two different waste sources were directly combined in the F10, F20, and F30 formulations. Their physicochemical characteristics were then correlated with BET pore parameters, CV response, and impedance behavior.

The comparison shows in **Table 6**, that the main contribution of the present study is the integrated evaluation of composition, accessible pore structure, and charge transport. F10 exhibited the highest total BET surface area, whereas F20 showed the highest

micropore surface area and micropore volume, the largest CV response, and the lowest $\Delta Z'$ among the investigated samples. Therefore, the results indicate that total surface area alone does not explain electrochemical performance. Nevertheless, because only three formulations were examined, F20 is identified as the best-performing formulation within the investigated range and not as a statistically determined global optimum.

Table 6. Comparison of previous studies on waste-derived electrode materials and the present study.

Study	Material	Research approach	Main focus	Difference from the present study
Wang et al. [16]	Coal fly ash	Fly ash was chemically transformed into cobalt–iron silicate and modified with carbon nanofibers	Supercapacitor electrode	Used chemical transformation rather than direct blending with MSWG char
Niu et al. [10]	Coal gasification fine slag	Residual carbon and mineral ash from one residue were formed into particle electrodes	Carbon–mineral electrocatalytic synergy	Used one gasification-waste source rather than two different waste materials
Guo et al. [11]	Coal gasification residual carbon	Carbon-rich fraction was prepared as an oxygen-reduction catalyst	Oxygen reduction reaction	Focused on the isolated carbon fraction rather than composition–pore–impedance correlation
Fernandes et al. [17]	Coal char recovered from fly ash	Char was processed through carbonization, demineralization, or graphitization	Oxygen-reduction electrocatalysis	Used processed fly-ash char rather than untreated mineral-rich coal fly ash
Nunes et al. [18]	Coal fly ash char	Fly-ash char was used as a partial graphite substitute	Oxygen-reduction activity	Did not combine coal fly ash with MSWG char
Present study	Coal fly ash and MSWG char	Direct comparative formulation of F10, F20, and F30	Correlation among raw-material characteristics, pore structure, CV, and EIS	Combines two waste sources and evaluates composition-dependent pore–transport behavior

A limitation of the present comparison is the absence of independently prepared experimental replicates. Consequently, variability associated with powder preparation, slurry mixing, electrode coating, cell assembly, and electrochemical measurement could not be quantified. The reported differences among F10, F20, and F30 therefore represent descriptive trends based on the available individual datasets and cannot be interpreted as statistically significant differences. Future studies should use at least three independently prepared electrodes per formulation, report the results as mean ± standard deviation, and apply an appropriate statistical analysis, such as one-way analysis of variance followed by a suitable post-hoc comparison, after verifying the assumptions of the selected test.

4. Conclusion

Initial characterization showed that coal fly ash and municipal solid waste gasification char have complementary roles. SEM–EDX revealed that coal fly ash had spherical or microsphere-like particles with high O, Si, and Al contents, indicating its role as a mineral-rich silicate and aluminosilicate precursor. In contrast, municipal solid waste gasification char showed irregular, rough, and agglomerated morphology with higher carbon content, making it the main carbon-phase source. FTIR confirmed that both materials contained silicate, oxide, hydroxyl, carbonate, and carbon–mineral bonding features. Comparative evaluation of the F10, F20, and F30 formulations identified F20 as the best-performing composition within the

investigated range. F20 showed the highest micropore surface area and volume, the largest CV response, an energy density of approximately 208 Wh kg^{-1}, a power density of 17.8 W kg^{-1}, and the lowest $\Delta Z'$ of 0.137 Ω. Because the formulation series consisted of only three compositions and was not developed using a Design of Experiments or statistical optimization procedure, F20 should not be interpreted as a global optimum. Future work should investigate intermediate compositions, such as F15 and F25, as well as compositions below 10 wt.% and above 30 wt.% coal fly ash, using replicated experiments and an appropriate statistical experimental design. Within the individual datasets evaluated, the results suggest that the observed electrode performance was associated with the combined effects of active-pore characteristics, electrolyte accessibility, and charge transport rather than with total BET surface area alone. Because independent experimental replicates were not available, the observed differences could not be evaluated statistically and should be interpreted as preliminary trends. Compared with previous studies that used chemically transformed fly ash, processed fly-ash char, or a single gasification residue, this study directly combined coal fly ash and MSWG char and correlated their composition with pore accessibility and charge-transport behavior. This study contributes to the utilization of MSWG char as a low-cost electrode material and supports circular-economy-based metal–air battery development.

Future investigations should prepare and evaluate at least three independent electrodes for each formulation, quantify the results using means and standard deviations, and apply appropriate statistical tests. Such replicated measurements are necessary to determine whether the observed differences are reproducible and statistically significant.

Author contributions: Conceptualization, methodology, formal analysis, investigation, data curation, and writing—review and editing, SP, RA, and MS; Software, resources, writing—original draft preparation, visualization, and project administration, SP; Validation and supervision, RA and MS. All authors have read and agreed to the published version of the manuscript.

Funding: This research was financially supported by the Alumni Foundation of Diponegoro University (Yayasan Alumni UNDIP) through the Doctoral Student Study Support Program 2023, awarded to Satria Pinandita.

Institutional review board statement: Ethical review and approval were not required for this study because it involved only material preparation, laboratory characterization, and electrochemical testing. No human participants, animals, or biological materials were involved.

Informed consent statement: Not applicable.

Data availability statement: The data supporting the findings of this study are available from the corresponding author upon reasonable request.

Acknowledgment: The authors would like to express their sincere gratitude to the Alumni Foundation of Diponegoro University (Yayasan Alumni UNDIP) for providing

financial support through the Doctoral Student Study Support Program 2023. The authors also gratefully acknowledge Universitas Semarang for its valuable assistance, facilities, and continuous support throughout the conduct of this research.

Conflict of interest: The authors declare that they have no known competing financial interests or personal relationships that could have appeared to influence the work reported in this paper.

AI use statement: During the preparation of this work, the authors used ChatGPT (OpenAI) for language editing, grammar improvement, and manuscript refinement. The authors subsequently reviewed and edited the content as necessary and take full responsibility for the final content of the published article.

Abbreviation

Symbol/Abbreviation	Definition	Unit
BET	Brunauer–Emmett–Teller surface-area analysis	–
CMC	Carboxymethyl cellulose	–
CV	Cyclic voltammetry	–
D_{avg}	Average pore diameter	nm
EDX	Energy-dispersive X-ray spectroscopy	–
EIS	Electrochemical impedance spectroscopy	–
Esp	Specific energy	Wh kg^{-1}
F10	Formulation containing 10 wt.% coal fly ash, 10 wt.% graphite, and 80 wt.% MSWG char in the hybrid powder mixture	–
F20	Formulation containing 20 wt.% coal fly ash, 10 wt.% graphite, and 70 wt.% MSWG char in the hybrid powder mixture	–
F30	Formulation containing 30 wt.% coal fly ash, 10 wt.% graphite, and 60 wt.% MSWG char in the hybrid powder mixture	–
f	Frequency	Hz
FTIR	Fourier-transform infrared spectroscopy	–
MSWG	Municipal solid waste gasification	–
NMC	Nickel–manganese–cobalt oxide	–
NMC 111	Nickel–manganese–cobalt oxide with an approximate Ni:Mn:Co ratio of 1:1:1	–
NMP	N-Methyl-2-pyrrolidone	–
ORR	Oxygen reduction reaction	–
Psp	Specific power	W kg^{-1}
PVDF	Polyvinylidene fluoride	–
SBR	Styrene–butadiene rubber	–
SEM	Scanning electron microscopy	–
S_{BET}	BET specific surface area	m^2 g^{-1}
S_{micro}	Micropore surface area	m^2 g^{-1}
V_{total}	Total pore volume	cm^3 g^{-1}
V_{micro}	Micropore volume	cm^3 g^{-1}
Z'	Real component of impedance	Ω
Z''	Imaginary component of impedance	Ω

$\|Z\|$	Impedance magnitude	Ω
$\Delta Z'$	Difference between the selected low- and high-frequency real-impedance values	Ω
θ	Impedance phase angle	°
Na_2CO_3	Sodium carbonate	–

References

1. Rai S, Prachi P, Kant CR, et al. Metal-air batteries: From fundamental mechanisms to practical applications. Journal of Alloys and Compounds. 2025; 1033: 180805. doi: 10.1016/j.jallcom.2025.180805
2. Timofeeva EV, Segre CU, Pour GS, et al. Aqueous air cathodes and catalysts for metal–air batteries. Current Opinion in Electrochemistry. 2023; 38: 101246. doi: 10.1016/j.coelec.2023.101246
3. Hopkins BJ, Chervin CN, Parker JF, et al. Electrocatalyst or support? Circumventing corrosion for long-lived zinc–air batteries. Next Energy. 2023; 1(4): 100054. doi: 10.1016/j.nxener.2023.100054
4. Gao S, Li M, Li N, et al. Porous carbon-nanostructured electrocatalysts for zinc–air batteries: from materials design to applications. Nanoscale Advances. 2025; 7(1): 60–88. doi: 10.1039/D4NA00847B
5. Supiyeva Z, Pan X, Abbas Q. The critical role of nanostructured carbon pores in supercapacitors. Current Opinion in Electrochemistry. 2023; 39: 101249. doi: 10.1016/j.coelec.2023.101249
6. Liu H, Zhang L. Pore-structure control of porous carbon electrode materials and energy-storage performance in water-in-salt electrolytes. Journal of Electroanalytical Chemistry. 2024; 961: 118233. doi: 10.1016/j.jelechem.2024.118233
7. Chai Y, Hu Z, Jia W, et al. Ion transport in porous carbon electrode for supercapacitors probed by electrochemical quartz crystal microbalance. Electrochimica Acta. 2020; 356: 136780. doi: 10.1016/j.electacta.2020.136780
8. Christopher Selvam D, Devarajan Y, Raja T, et al. Advances in waste-derived nano-catalysts for zinc–air batteries: Enhancing OER efficiency and sustainability in energy storage. Applied Energy. 2025; 400: 126605. doi: 10.1016/j.apenergy.2025.126605
9. He T, Tian H, Hong J, et al. From hazardous waste to high-performance anodes: Iron-Catalyzed upcycling of coal gasification slag into hierarchical porous carbon for sodium-ion batteries. Fuel. 2026; 404: 136320. doi: 10.1016/j.fuel.2025.136320
10. Niu Y, Chen L, Guo S, et al. Porous carbon/minerals interwoven particle electrodes co-constructed by residual carbon and ash from coal gasification fine slag and its synergistic electrocatalytic mechanism. Fuel. 2024; 358: 130139. doi: 10.1016/j.fuel.2023.130139
11. Guo Q, Li H, Wang S, et al. Experimental study on preparation of oxygen reduction catalyst from coal gasification residual carbon. Chemical Engineering Journal. 2022; 446: 137256. doi: 10.1016/j.cej.2022.137256
12. Ma C, Fan Q, Dirican M, et al. Rational design of meso-/micro-pores for enhancing ion transportation in highly-porous carbon nanofibers used as electrode for supercapacitors. Applied Surface Science. 2021; 545: 148933. doi: 10.1016/j.apsusc.2021.148933
13. Witte A, Garg N. Particle shape, crystallinity, and degree of polymerization of fly ash via combined SEM-EDS and Raman spectroscopy. Cement and Concrete Research. 2024; 184: 107612. doi: 10.1016/j.cemconres.2024.107612
14. Kutchko B, Kim A. Fly ash characterization by SEM–EDS. Fuel. 2006; 85(17–18): 2537–2544. doi: 10.1016/j.fuel.2006.05.016
15. Bhatt A, Priyadarshini S, Acharath Mohanakrishnan A, et al. Physical, chemical, and geotechnical properties of coal fly ash: A global review. Case Studies in Construction Materials. 2019; 11: e00263. doi: 10.1016/j.cscm.2019.e00263
16. Wang H, Wang M, Zhang J, et al. Preparation of fly ash-based cobalt-iron silicate as supercapacitor electrode material. Chemical Engineering Journal. 2022; 434: 134661. doi: 10.1016/j.cej.2022.134661
17. Fernandes DM, Abdelkader-Fernández VK, Badenhorst C, et al. Coal chars recovered from fly ash as promising electrocatalysts for oxygen reduction reaction. International Journal of Hydrogen Energy. 2021; 46(70): 34679–34688. doi: 10.1016/j.ijhydene.2021.08.009
18. Nunes MS, Pereira C, Guedes A, et al. Assessment of coal fly ash char as a substituting material of graphite with electrocatalytic activity for the oxygen reduction reaction. Sustainable Chemistry and Pharmacy. 2022; 27: 100705.

doi: 10.1016/j.scp.2022.100705
19. Qin J, Zhang Y, Heberlein S, et al. Characterization and comparison of gasification and incineration fly ashes generated from municipal solid waste in Singapore. Waste Management. 2022; 146: 44–52. doi: 10.1016/j.wasman.2022.04.041
20. Wang B, Gupta R, Bei L, et al. A review on gasification of municipal solid waste (MSW): Syngas production, tar formation, mineral transformation and industrial challenges. International Journal of Hydrogen Energy. 2023; 48(69): 26676–26706. doi: 10.1016/j.ijhydene.2023.03.086
21. Sajid M, Raheem A, Ullah N, et al. Gasification of municipal solid waste: Progress, challenges, and prospects. Renewable and Sustainable Energy Reviews. 2022; 168: 112815. doi: 10.1016/j.rser.2022.112815
22. Saini R, Deb Barma S, Srinivas Rao D, et al. Applied mineralogical investigation on coal gasification ash. Waste Management. 2023; 167: 1–12. doi: 10.1016/j.wasman.2023.05.025
23. Wood DL, Li J, Daniel C. Prospects for reducing the processing cost of lithium ion batteries. Journal of Power Sources. 2015; 275: 234–242. doi: 10.1016/j.jpowsour.2014.11.019
24. Baig MM, Gul IH, Baig SM, et al. The complementary advanced characterization and electrochemical techniques for electrode materials for supercapacitors. Journal of Energy Storage. 2021; 44: 103370. doi: 10.1016/j.est.2021.103370
25. Beyers I, Bensmann A, Hanke-Rauschenbach R. Ragone plots revisited: A review of methodology and application across energy storage technologies. Journal of Energy Storage. 2023; 73: 109097. doi: 10.1016/j.est.2023.109097
26. Velraj S, Zhu JH. Cycle life limit of carbon-based electrodes for rechargeable metal–air battery application. Journal of Electroanalytical Chemistry. 2015; 736: 76–82. doi: 10.1016/j.jelechem.2014.11.003
27. Kang X. Critique on the "Crystallinity and selected properties of fly ash particles" by T. Matsunaga, J.K. Kim, S. Hardcastle, P.K. Rohatgi, Crystallinity and selected properties of fly ash particles, Materials Science and Engineering A, Volume 325, Issues 1–2, 28 February 2002, Pages 333–343. Materials Science and Engineering: A. 2014; 613: 414. doi: 10.1016/j.msea.2014.07.019
28. Ismael MA, Aziz ARA, Zainal A. EZ, et al. Investigation on free-piston motion and power generation of a dual-piston air-driven expander linear generator. Energy Reports. 2021; 7: 2388–2397. doi: 10.1016/j.egyr.2021.04.035
29. Qian Y, Liu J, Huang Z, et al. Conceptual design and system analysis of a poly-generation system for power and olefin production from natural gas. Applied Energy. 2009; 86(10): 2088–2095. doi: 10.1016/j.apenergy.2008.12.014
30. Huang J. Diffusion impedance of electroactive materials, electrolytic solutions and porous electrodes: Warburg impedance and beyond. Electrochimica Acta. 2018; 281: 170–188. doi: 10.1016/j.electacta.2018.05.136
31. Wang M, Chen D, Wang H, et al. A review on fly ash high-value synthesis utilization and its prospect. Green Energy and Resources. 2024; 2(1): 100062. doi: 10.1016/j.gerr.2024.100062
32. Widayat W, Maheswari NT, Fitriani W, et al. Preparation of MgO-CaO/SiO_2 catalyst from dolomite and geothermal solid waste for biodiesel production. International Journal of Renewable Energy Development. 2023; 12(3): 541–549. doi: 10.14710/ijred.2023.51573
33. Konda K, Moodakare SB, Kumar PL, et al. Comprehensive effort on electrode slurry preparation for better electrochemical performance of $LiFePO_4$ battery. Journal of Power Sources. 2020; 480: 228837. doi: 10.1016/j.jpowsour.2020.228837
34. Zhuang B, Xu N, Xu X, et al. Hierarchically mesoporous Fe-N-C single-atom catalysts for efficient oxygen electrocatalysis in rechargeable zinc-air batteries. Materials Reports: Energy. 2025; 5(3): 100352. doi: 10.1016/j.matre.2025.100352
35. Chen T, Huang S, Pei X, et al. Synergistic Co/Cu heterophase nanoparticles embedded in microporous and mesoporous carbon with hydrophobicity for high-power density zinc-air battery. Electrochimica Acta. 2025; 530: 146336. doi: 10.1016/j.electacta.2025.146336
36. Liivand K, Sainio J, Wilson BP, et al. Overlooked residue of Li-ion battery recycling waste as high-value bifunctional oxygen electrocatalyst for Zn-air batteries. Applied Catalysis B: Environmental. 2023; 332: 122767. doi: 10.1016/j.apcatb.2023.122767
37. Shen Z, Yu X, Yu D. Preparation and applications of coal fly ash-based catalysts: A comprehensive review. Journal of Environmental Chemical Engineering. 2025; 13(3): 116782. doi: 10.1016/j.jece.2025.116782
38. Lasia A. Impedance of porous electrodes. Current Opinion in Electrochemistry. 2025; 54: 101764. doi: 10.1016/j.coelec.2025.101764
39. Subbiah G, Nagappan B, Sharma S, et al. Pioneering advances in waste-derived catalysts for next-generation zinc-air batteries. Results in Engineering. 2025; 27: 106161. doi: 10.1016/j.rineng.2025.106161

40. Tao F, Liu Y, Ren X, et al. Different surface modification methods and coating materials of zinc metal anode. Journal of Energy Chemistry. 2022; 66: 397–412. doi: 10.1016/j.jechem.2021.08.022
41. Mollah MYA, Hess TR, Cocke DL. Surface and bulk studies of leached and unleached fly ash using XPS, SEM, EDS and FTIR techniques. Cement and Concrete Research. 1994; 24(1): 109–118. doi: 10.1016/0008-8846(94)90091-4
42. Liu J, Li X, Jin B, et al. Optimizing porous structure of carbon electrodes for temperature-independent capacitance at sub-zero temperatures. Chemical Engineering Journal. 2022; 441: 136053. doi: 10.1016/j.cej.2022.136053